ADVANCED MATERIALS

DOI: 10.1002/adma.200600213

High-Density Arrays of Germanium Nanowire Photoresistors**

By *Boris Polyakov*, *Brian Daly*, *Juris Prikulis*, *Vaclovas Lisauskas*, *Bonifacas Vengalis*, *Michael A. Morris*, *Justin D. Holmes*,* and *Donats Erts**

Here we present for the first time a study of the photoresistive properties and dynamics of ordered, high-density arrays of germanium nanowire photoresistors. Germanium is a well-known semiconducting material with an indirect bandgap, E_g, of approximately 0.66 eV (temperature $T = 300$ K)[1] and has been widely used for the fabrication of photodetectors,[2–5] radiation detectors,[6–8] charged particle and photon tracking devices,[9] far-infrared photoresistors,[10] and numerous other devices.[11] During the last few years there has also been increasing interest in the use of nanostructures (quantum dots and wires) of both germanium and silicon as materials for potential applications in sensors, nanophotonics, and nanoelectronics.[12–14] However, in order to successfully integrate one-dimensional semiconductors into useful devices, ordered architectures of aligned nanowires are required. Using templates such as anodized aluminium oxide (AAO)[15,16] or mesoporous materials[17,18] as hosts for nanowires offers a viable method for forming high-density arrays of ordered, crystalline nanowires. Significantly, AAO membranes with ordered and highly oriented pore structures have recently been synthesized on silicon substrates,[19,20] which is very promising for the integration of such materials into current complementary metal oxide semiconductor technologies. At University College Cork we have developed supercritical-fluid-inclusion phase methods for forming semiconductor[21–23] and metal/semiconductor core/shell[24] nanowires and nanotubes within the pores of mesoporous matrices and AAO membranes. Supercritical-fluid-inclusion methods are ideal solvents for forming high-density arrays of nanowires within AAO templates as they do not suffer from the inherent problem of pore blocking associated with other methods, such as electrodeposition and incipient wetness techniques.

The electrical conductivity and photoluminescence properties of semiconductor nanowire arrays have been investigated by several research groups.[25–28] However, photoconductivity measurements on ordered semiconducting nanowire arrays have not yet been performed. An investigation into the photoconductivity of ordered arrays of nanowires is important in order to fully understand their potential in future photodetection devices, for example, as photoresistors or photodiodes. In this paper, we report the photoconductive properties of germanium nanowire photoresistors with mean diameters of 50 and 100 nm, incorporated within the pores of AAO membranes. A comparative study of the photoresistive properties of germanium nanowire photoresistor arrays with different optically transparent electrodes, namely ultrathin gold films and tin-doped indium tin oxide (ITO) layers, is described in this paper. ITO is a well known n-type semiconductor widely used in the fabrication of transparent electrodes in various optoelectronic devices.[29] To our knowledge, this study is the first analysis of photoconductivity in ordered semiconducting nanowire arrays.

Germanium nanowires, with mean diameters of 50 and 100 nm were synthesized in the pores of AAO membranes. The electrical and structural properties of these Ge nanowire arrays has previously been reported[28] (see Supporting Information). Figure 1a shows a current-distribution map of the encapsulated nanowires, with a mean diameter of 100 nm, obtained using conductive atomic force microscopy (C-AFM). Practically all of the Ge nanowires incorporated within the AAO membranes demonstrated similar electrical conductiv-

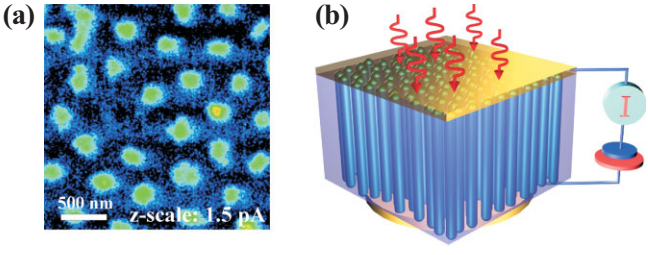

Figure 1. a) Current map of the top surface of a 100 nm Ge–AAO sample at 25 V. b) Schematic drawing of the photoconductivity measurement assembly.

[*] Dr. J. D. Holmes, Dr. D. Erts, B. Daly, Prof. M. A. Morris
Department of Chemistry, Materials Section and
Supercritical Fluid Centre
University College Cork (Ireland)
E-mail: j.holmes@ucc.ie; Donats.Erts@lu.lv
Dr. J. D. Holmes, Dr. D. Erts, B. Daly, Prof. M. A. Morris
Centre for Research on Adaptive Nanostructures and Nanodevices (CRANN), Trinity College Dublin
Dublin 2 (Ireland)
Dr. D. Erts, B. Polyakov, Dr. J. Prikulis
Institute of Chemical Physics, University of Latvia
LV-1586 Riga (Latvia)
Dr. V. Lisauskas, Dr. B. Vengalis
Institute of Semiconductor Physics
LT-01108, Vilnius (Lithuania)

[**] The authors acknowledge financial support for their work from the Council of Science of Latvia, University of Latvia, the Irish Research Council for Science and Engineering (IRCSET) and the Centre for Research on Adaptive Nanostructures and Nanodevices (CRANN). B. Polyakov and J. Prikulis acknowledge financial support from the European Social Fund. Supporting Information is available online from Wiley InterScience or from the author.

ity when individually probed using C-AFM at 25 V.[28] Green areas on the conductivity map indicate current flow through the nanowires, while the dark areas demonstrate the absence of current passing through the AAO matrix. Figure 1b illustrates a schematic of the photoconductivity assembly used in these experiments. Ge nanowires incorporated within the AAO membranes were polished and etched to expose the ends of the nanowires. To perform photoconductivity measurements, the top surface of the AAO–nanowire membranes were coated with an optically transparent conductive ITO electrode or semitransparent Au coating (thickness, $d \sim 25$ nm). A Au film ($d \sim 100$ nm), 1 mm in diameter, was used as a bottom electrode.

Figure 2a shows dark current–voltage (*IV*) curves measured at room temperature for arrays of Ge nanowires formed within the AAO templates. The *IV* curves were measured by passing a current between the transparent ITO top electrode and the bottom Au electrode. Curves 1 and 3, displayed in Figure 2a, correspond to Ge nanowires with mean diameters of 50 and 100 nm, respectively. With these samples the ITO electrode was deposited directly onto the surface of the polished Ge nanowires–AAO membranes. Curves 2 and 4 were obtained for arrays of Ge nanowires with mean diameters of 50 and 100 nm, respectively, where the surface of the AAO was etched back by approximately 100 nm with phosphoric acid to expose the tops of the Ge nanowires before the ITO electrode was deposited. Etching times of between 15 and 45 min and 3 and 10 min were used for the Ge nanowire–AAO samples with mean nanowire diameters of 100 and 50 nm, respectively.

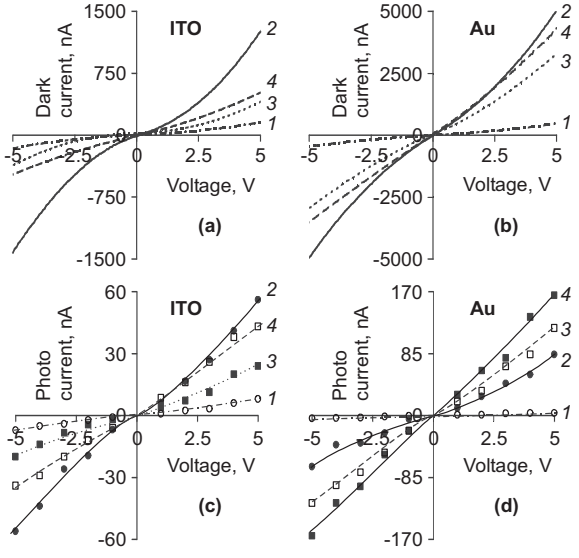

Figure 2. *IV* characteristics of Ge nanowire–AAO samples with mean diameters of 50 and 100 nm: a) dark currents from deposited ITO top electrodes, b) dark currents from semitransparent Au top electrodes (thickness ca. 25 nm), c) photocurrent, I_{ph} from deposited ITO electrodes, and d) I_{ph} from semitransparent Au electrodes obtained using a laser intensity of 800 mW cm^{-2} measured after 50 ms illumination. Plots 1 and 3: *IV* data from Ge nanowires with mean diameters of 50 and 100 nm, respectively, after polishing of the AAO surface before contact deposition. Plots 2 and 4: *IV* data from Ge nanowires with mean diameters of 50 and 100 nm, respectively, after polishing and etching of the AAO membranes before electrode deposition.

The dark *IV* characteristics of the Ge nanowires within the AAO templates were also measured using semitransparent Au electrodes instead of ITO electrodes. The respective *IV* curves are shown in Figure 2b. The significance of the contact resistance between the optically transparent top ITO (Au) and bottom Au contact and the Ge nanowires can be deduced from the *IV* data shown in Figure 2a and b. A higher electrical resistance was obtained for the polished nanowire samples than for the polished and chemically etched nanowire–AAO samples. Polishing and etching of the samples was observed to result in a reduction of the measured sammple resistance by a factor of ten for nanowires with a mean diameter of 50 nm, and by approximately 50 % for nanowires with a mean diameter of 100 nm, compared to "polished only" samples, as shown in Figure 2a and b and Table 1. This significant decrease in resistance observed for the 50 nm nanowires after etching is probably due to a large increase in the exposed contact area of the nanowires. For example, taking into account the density

Table 1. Resistance of a single nanowire estimated for various Ge nanowire–AAO samples after different contact preparations.

Sample	Resistance [Ω] ITO contact	Resistance [Ω] Semitransparent Au contact
Polished 50 nm GeNW–AAO	2×10^{15}	6.6×10^{14}
Polished and etched 50 nm GeNW-AAO	2.3×10^{14}	6×10^{13}
Polished 100 nm GeNW–AAO	8.8×10^{13}	1.1×10^{13}
Polished and etched 100 nm GeNW–AAO	6.4×10^{13}	8.4×10^{12}

of nanowires within the AAO templates, that is, 1.4×10^{10} and 9×10^{8} cm^{-2} for 50 and 100 nm diameter nanowires respectively, and assuming that in both cases each nanowire extends above the etched AAO surface by approximately 100 nm, one can estimate that additional chemical etching results in an increase of the contact area under a 1 mm diameter electrode from 0.22 to approximately 2 mm^2 for the 50 nm nanowires and from 0.057 to 0.28 mm^2 for the 100 nm diameter nanowires. The data presented in Figure 2a and b and Table 1 show that the resistance of the etched samples with ITO coatings was a factor of eight greater than Au-coated samples. The observed higher resistance of the ITO-coated samples may be explained by partial oxidation of Ge nanowires during ITO coating in an O_2-containing atmosphere.

An increase in the current was observed for the Ge nanowire–AAO samples during illumination with an Ar laser with an intensity of 800 mW cm^{-2}, a wavelength range between 457 and 514 nm, and a pulse of 0.5 ms, for both the ITO and semitransparent top Au electrodes. Figure 2c and d show the photocurrent (I_{ph}), $I_{ph} = I_t - I_d$, where I_d and I_t are the dark current and total current, respectively, as a function of applied voltage for the Ge nanowire samples. No photocurrent was

ADVANCED MATERIALS

detected in the empty AAO membranes, that is, those not loaded with Ge nanowires in the pores. The $I_{ph}V$ curves displayed in Figure 2c and d for the 50 and 100 nm diameter Ge nanowires are similar to the dark current versus voltage plots displayed for the same samples in Figure 2a and b.

The photocurrent/dark current ratio (I_{ph}/I_d) was typically 10–25 % for the ITO–nanowire and 3–5 % for the Au–nanowire contacts, for both the chemically etched and nonetched samples. The difference in the I_{ph}/I_d ratios is mainly due to the lower transparency of the top Au contact compared to the ITO electrode. The light intensity decreases by approximately 50 % after passing light through a 25 nm thick Au-coated film on a glass substrate in our test experiments. As ITO is transparent, the loss of light due to reflection and absorption is negligible. Photocurrent versus light intensity dependence was found to be linear for the Ge nanowire–AAO samples for both the ITO and Au contacts in the interval of 100 to 800 mW cm^{-2} for both the etched and nonetched samples. Thus, taking into account the low intensity of light transmitted through the Au electrode, the Au- and ITO-coated samples show practically the same I_{ph}/I_d ratios.

Bearing in mind the photocurrents shown in Figure 2c and d and the nanowire densities, we estimate that for the semitransparent Au electrode the photocurrent in a single Ge nanowire, at a bias of 5 V and illumination power of 800 mW cm^{-2}, is in the range of 30 fA for the 100 nm and 3 fA for the 50 nm nanowires. The photocurrent increases linearly with bias voltage and is ten times higher at 50 V compared to that at 5 V. This indicates that individual Ge nanowire photoresistors within the AAO templates demonstrate a sufficient photoinduced current effect that can be used in devices based on nanowires with high lateral resolution.

The photocurrent dynamics in the nanowire–AAO arrays measured at room temperature are shown in Figure 3. The samples displayed exponential growth and decay kinetics with time constants (τ_i) ranging from sub-milliseconds to seconds. Mathematically the time dependence can be expressed as shown in Equation 1 below:

$$I_{total}(t) = I_0 \pm \sum_i C_i \cdot \exp(-t/\tau_i) \quad (1)$$

where I_{total} is the current detected after a time t, I_0 is the steady current at a given illumination intensity, C_i is a numerical coefficient, and τ_i is the current change time constant. The estimated time constants from the experimental data were found to vary slightly with nanowire diameter and electrode material but did not vary between nonetched and etched samples (Table 2).

The nanowire–AAO membranes displayed photocurrent kinetics on the millisecond timescale, as shown in Figure 3a. The kinetics consist of two components. The first kinetic time constant (τ_1) is too short to be determined by the 0.5 ms pulse used in our experiments but is faster than 10^{-4} s, as can be seen in the pulse decay front in Figure 3a. The time constants of the second kinetic component (τ_2) are around 10^{-3} s (Fig. 3a, Table 2). The first kinetic component can be attributed to photoprocesses in the Ge nanowires. For comparison,

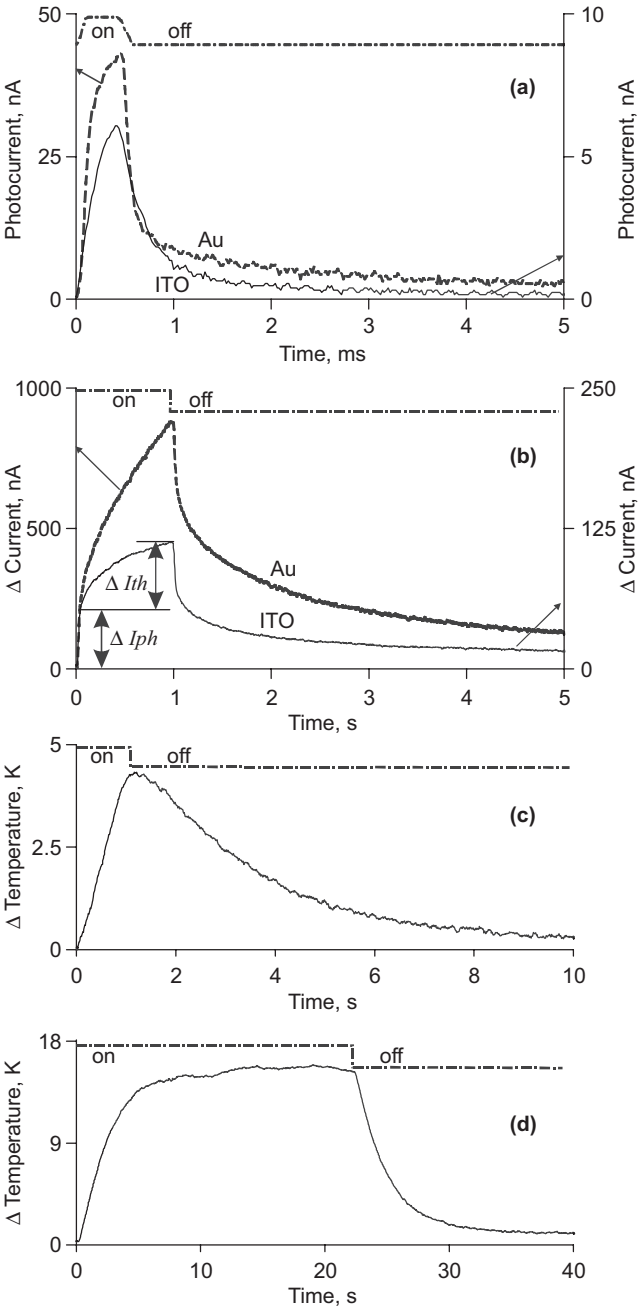

Figure 3. a,b) The photocurrent dynamics of etched arrays of Ge nanowires with mean diameters of 100 nm: a) at 0.5 ms laser pulse illumination for Au and ITO electrodes, b) at 1 s for Au and ITO electrodes (Impacts of photogenerated and thermogenerated currents are shown as ΔI_{ph} and ΔI_{th}). Plots obtained for arrays of Ge with mean diameters of 50 nm were very similar. c) The 100 nm pore diameter Ge nanowire array sample temperature dynamics after heating for 1 s. d) Heating dynamics for the same sample during prolonged illumination (22 s). The top line indicates laser pulse duration (on-off). Laser light intensity was 800 mW cm^{-2} in all cases.

Table 2. Characteristic time constants estimated in this work for Ge nanowire–AAO samples.

Nanowire diameter [nm]	Electrode	τ_1 [ms]	τ_2 [ms]		τ_3 [s]	
			increase	decrease	increase	decrease
50	ITO	<0.1	0.4–0.5	1–3	2–3	0.5–4
50	25 nm Au	<0.1	0.4–4	3–7	0.5–1	2–2.5
100	ITO	<0.1	0.25–0.5	0.8–2	1.5–5	1–1.4
100	25 nm Au	<0.1	0.4–0.8	0.5–4	1–1.5	1.7

charge-carrier lifetimes in polycrystalline bulk Ge are around 3×10^{-6} s.[30] The second kinetic component (τ_2) may be associated with the presence of charge traps in the Ge nanowires or from photoluminescence processes in the AAO matrix, which have approximately the same measured photoluminescence time constant.

For longer illumination pulses, a third kinetic component with a time constant of $\tau_3 = 0.5$–4 s was observed (Fig. 3b and Table 2). This kinetic component is due to thermogenerated current due to sample heating upon laser illumination. The sample heating was directly measured using a thermocouple attached to the back side of the Ge nanowire–AAO membranes. At the shortest illumination pulses (0.5 ms), the rise in sample temperature was negligible (10^{-3} K). At longer illumination times, the temperature increased and decreased linearly with time as $T(t) \sim t/\tau_{th}$ within the first 1–2 s (Fig. 3c) and stabilized after about 10 s, as shown in Figure 3d. The close correlation between the current and temperature kinetics (τ_3 and τ_{th}) suggests that the current kinetics are solely determined by sample heating. The current through the Ge nanowires inside the AAO membranes was found to depend exponentially on temperature, $I \sim \exp(-1/T)$, as was reported in our previous work.[28] Thus, the linear growth of the sample temperature during sample illumination (Fig. 3c) causes an exponential increase in current $I(t) \sim \exp(-t/\tau_{th})$ approximately 0.1 s after illumination starts, and is marked as thermocurrent (ΔI_{th}) in Figure 3b. In the first 0.1 s of illumination, the current increases exponentially. The time constant in this region (marked ΔI_{ph}) is at least three orders of magnitude faster that the time constant in the region marked (ΔI_{th}) (Fig. 3b), and corresponds to the fast kinetic component (τ_1 and τ_2) (Fig. 3a). Therefore, we attribute the current in the region marked (ΔI_{ph}) to photocurrent and the current in the region marked (ΔI_{th}) to temperature-induced current. Therefore, it is possible to separate the photo- and thermoinduced effects by analyzing the photokinetics when longer illumination times are used.

In summary, we have demonstrated that ITO and semitransparent Au act as effective electrodes for measuring the photoconductivities of Ge nanowire arrays. Improvements in contact resistance between the electrodes and the nanowires was achieved by mechanically polishing and chemically etching the membranes. Photoinduced conductivity in Ge nanowire arrays, with mean nanowire diameters of 50 and 100 nm, was demonstrated. The work reported in this paper therefore offers a viable method for the use of Ge nanowire arrays as photoresistors and as potential architectures for photoelectronic devices.

Experimental

Ge nanowires were synthesized within the pores of AAO membranes using a supercritical fluid flow-through deposition system, as described previously [31]. The surfaces of the Ge nanowire–AAO membrane were mechanically polished using three diamond suspensions with grain sizes of 6.0, 1.0, and 0.25 μm. After polishing, the membranes were washed with acetone. Ge nanowires protruding from the surface of the AAO were observed using AFM. The density of Ge nanowires within the AAO membranes was 9×10^8 and 1.4×10^{10} nanowires cm^{-2} for mean pore diameters of 100 and 50 nm, respectively. The Ge nanowires within the AAO templates, with lengths between 40 and 60 μm, were found to be conductive and exhibit intrinsic conductivity properties, as previously reported [27,28].

To perform photoconductivity measurements, the top surface of the AAO membranes was coated with an optically transparent conductive ITO electrode or semitransparent Au coating ($d \sim 25$ nm). Meanwhile, a nontransparent ($d \sim 100$ nm) Au electrode, 1 mm in diameter, was used as a bottom electrode (see schematic drawing in Fig. 1). The ITO contacts were prepared either on a mechanically polished or chemically etched surface by DC magnetron sputtering using a disk-shaped metallic $In_{91}Sn_9$ target. Sputtering was conducted for 20 min in an argon/oxygen (20:1) atmosphere at a pressure of 4 Pa keeping the substrate temperature at 250 °C. Voltage and discharge current during the deposition were 300 V and 50 mA, respectively. The top and bottom Au coatings were deposited in vacuum ($P = 10^{-4}$ Torr. 1 Torr ≈ 133 Pa) at a deposition rate of about 1.7 Å s^{-1} using a precision etching coating system (Gatan). To remove surface contamination and possible oxide layers from the surface of the nanowires before Au deposition, the samples were cleaned for 20 s using Ar ions with an energy of 5 keV.

The sample surface coated with ITO or the semitransparent Au layer was illuminated by a 100 mW Melles Griot multimode Ar laser ($\lambda = 457$–514 nm). Current passing through the samples was measured at room temperature using a low-noise current amplifier SR570 (Stanford Research Systems). The sample temperature was measured using a copper–constantan thermocouple, attached to the back side of the sample silver paste. Laser light was introduced using a Nikon photographic camera, which was used as a mechanical shutter for measurements from the millisecond to second timescale.

Received: February 2, 2006
Final version: April 20, 2006
Published online: June 21, 2006

[1] S. M. Sze, *Physics of Semiconductor Devices*, Wiley, New York **1981**.
[2] J. Piprek, *Semiconductor Optoelectronic Devices: Introduction to Physics and Simulation*, Academic, Boston **2003**.
[3] P. N. J. Dennis, *Photodetectors an Introduction to Current Technology*, Plenum, New York **1986**.
[4] J. Piotrowski, *Opto-Electron. Rev.* **2004**, *12*, 111.
[5] A. I. Yakimov, A. V. Dvurechenskii, A. I. Nikiforov, Y. Y. Proskuryakov, *J. Appl. Phys.* **2001**, *89*, 5676.
[6] C. F. G. Delaney, E. C. Finch, *Radiation Detectors Physical Principles and Applications*, Clarendon, Oxford **1992**.
[7] G. Lutz, *Semiconductor Radiation Detectors Device Physics*, Springer, Berlin **1999**.
[8] P. Rehak, *IEEE Trans. Nucl. Sci.* **1999**, *51*, 2492.
[9] M. A. Deleplanque, I. Y. Lee, K. Vetter, G. J. Schmid, F. S. Stephens, R. M. Clark, R. M. Diamond, P. Fallon, A. O. Macchiavelli, *Nucl. Instrum. Methods Phys. Res., Sect. A* **1999**, *430*, 292.

[10] G. H. Rieke, *Detection of Light*: *From the Ultraviolet to the Submillimeter*, Cambridge University Press, Cambridge **1994**.
[11] N. T. Ranger, *Radiographics* **1999**, *19*, 481.
[12] L. J. Lauhon, M. S. Gudiksen, D. Wang, C. M. Lieber, *Nature* **2002**, *420*, 57.
[13] Y. Wu, R. Fan, P. Yang, *Nano Lett.* **2002**, *2*, 83.
[14] Y. Wu, P. Wang, *Chem. Mater.* **2000**, *12*, 605.
[15] H. Masuda, M. Satoh, *Jpn. J. Appl. Phys.*, *Part 1* **1993**, *35*, 126.
[16] H. Masuda, K. Fukuda, *Science* **1995**, *268*, 1466.
[17] S. Banderjee, A. Dan, D. Chakrovorty, *J. Mater. Sci.* **2002**, *37*, 4261.
[18] Z. Zhang, S. Dai, A. Blom, J. Shen, *Chem. Mater.* **2002**, *14*, 965.
[19] O. Rabin, P. R. Herz, Y. M. Lin, A. I. Akinwande, S. B. Cronin, M. L. Dresselhaus, *Adv. Funct. Mater.* **2003**, *13*, 631.
[20] M. Tian, S. Xu, J. Wang, N. Kumar, E. Wertz, Q. Li, P. M. Campbell, M. H. W. Chan, T. E. Mallouk, *Nano Lett.* **2005**, *5*, 697.
[21] K. M. Ryan, D. Erts, H. Olin, M. A. Morris, J. D. Holmes, *J. Am. Chem. Soc.* **2003**, *125*, 6284.
[22] D. M. Lyons, K. M. Ryan, M. A. Morris, J. D. Holmes, *Nano Lett.* **2002**, *2*, 811.
[23] N. R. B. Coleman, M. A. Morris, T. R. Spalding, J. D. Holmes, *J. Am. Chem. Soc.* **2001**, *123*, 187.
[24] T. A. Crowley, B. Daly, M. A. Morris, O. Kazakova, D. Erts, J. J. Boland, B. Wu, J. D. Holmes, *J. Mater. Chem.* **2005**, *15*, 2408.
[25] G. Audoit, E. Ní Mhuircheartaigh, S. M. Lipson, M. A. Morris, W. J. Blau, J. D. Holmes, *J. Mater. Chem.* **2005**, *15*, 4725.
[26] J. F. Qi, A. M. Belcher, J. M. White, *Appl. Phys. Lett.* **2003**, *82*, 2616.
[27] K. J. Ziegler, B. Polyakov, J. S. Kulkarni, T. A. Crowley, K. M. Ryan, M. A. Morris, D. Erts, J. D. Holmes, *J. Mater. Chem.* **2004**, *14*, 585.
[28] D. Erts, B. Polyakov, B. Daly, M. A. Morris, S. Ellingboe, J. J. Boland, J. D. Holmes, *J. Phys. Chem. B* **2006**, *110*, 820.
[29] I. Hamberg, C. G. Granqvist, *J. Appl. Phys.* **1986**, *60*, R123.
[30] H. Watakabe, T. Sameshima, H. Kanno, M. Miyao, *Thin Solid Flms*, in press.
[31] T. A. Crowley, K. J. Ziegler, D. M. Lyons, D. Erts, H. Olin, M. A. Morris, J. D. Holmes, *Chem. Mater.* **2003**, *15*, 3518.

